Influence of Protrusion Effect on the Accuracy of the Acoustic Discharge Measurement

Peter Gruber
Rittmeyer Ltd., Baar
Switzerland
peter.gruber@hslu.ch

Thomas Staubli
HSLU T&A, Lucerne
Switzerland
thomas.staubli@hslu.ch

Fabian Wermelinger
HSLU T&A, Lucerne
Switzerland
fabian.wermelinger@hslu.ch

Fabian Deschwanden
HSLU T&A, Lucerne
Switzerland
fabian.deschwanden@stud.hslu.ch

Abstract

The influence of the protrusion effect has gained in importance because of the introduction of multipath Acoustic Transit time (ATT) installations with a high number of paths. The transducers of the outermost paths tend to protrude in these cases much more into the pipe in order to be aligned correctly. Therefore its influence has to be estimated by taking its position into account. Protrusion effects caused by wetted acoustic transducers are twofold: 1) Overestimation of the mean path velocities due to the fact that the smaller velocities of the boundary layer are not taken into account when the mean path velocity is evaluated from sensor pill to sensor pill. This phenomenon is termed *reduced path length effect*. 2) The distortion of the velocity profile due to the protrusion of the transducer. This effect is different for the two adjacent sensors and can lead to underestimation. This phenomenon is termed *flow field distortion effect*. The first effect has been described by SUGISHITA et al. [3] for the NIKURADSE profile and center paths. This paper extends the formula of SUGISHITA to general velocity profiles and path positions. Correction diagrams are shown for different profiles and sensor positions in function of the protrusion depth. The mathematical facility derived in this paper to calculate these *geometrical* corrections can generally be used to calculate the geometrical properties of any acoustic path contained in a circular conduit. The second effect is determined by CFD simulations for specific transducer types. The goal of the paper is to specify bounds on the influence in function of the ratio protrusion depth to path length.

1 Introduction

If the **A**coustic **D**ischarge **M**easurement (ADM) based on the transit time method (ATT) is used for the determination of the flow in *circular* conduits, different error sources contribute to an overall measurement uncertainty. There are the following sources:

Flow determination error due to the determination of the flow Q. This error contains timing errors for the determination of the transit times and transit time difference as well as geometrical errors in the measurement of the geometrical quantities like path lengths, path angles and pipe geometry. The measured times and geometrical quantities are then used for the determination of the velocity according to the formula:

$$\overline{v}_{ax} = \frac{L}{2\cos\varphi}\left(\frac{1}{t_d} - \frac{1}{t_u}\right) \tag{1}$$

Integration error due to the integration of the actual velocity field. This error includes all the inaccuracies introduced by the numerical integration of the velocity field via a weighted sum of a number of discrete mean path velocities. This error depends on the hydraulic conditions and the chosen integration method[1].

Protrusion error due to the protrusion effect of the installed transducers. This error is dependent on the transducer geometry, pipe size respectively path length and the flow condition (velocity profile).

Ambient error due to the ambient influences of temperature, pressure and other water conditions

Clamp-on systems do not have protrusion error problems but suffer from other additional major error sources and are therefore not included in ADM systems for accurate flow measurement. In this study, only the protrusion error is examined. Estimates for the range of its magnitude are derived. An ADM system can be installed in two ways depending on the site specific situation:

- The transducers are mounted by drilling holes through the pipe wall. In this case the positions of the sensor pill surfaces are dependent on the transducer type and on how much the transducers are screwed in. Usually the positions are such that the centres of the sensor pills are located inside the pipe by a small value (less than 1-2cm).
- The transducers are mounted from the inside. In this case the positions of the centre of the sensor pills are only dependent on the transducer type and are located always inside the pipe by a transducer specific more or less constant value. This value can be as big as 5cm.

If the transducers protrude inside the fluid flow, they reduce the path length from pill to pill and they distort the velocity field. Both effects have an influence on the calculation of the mean path velocity. The amount is, as noted earlier, dependent on the transducer geometry, the path positions, path lengths and the velocity profile $\overline{v}_{ax}$ at the fixed coordinate y.

Reduced path length effect The protruding transducers shorten the acoustic path length from pill to pill due to its physical dimensions. The portions of the velocity field close to the pipe wall will be ignored. As every velocity profile is such that it is decreasing towards zero close to the pipe wall, the resulting measured mean path velocities will always be *higher* in magnitude than the actual mean path velocity. This correction factor for the i-th path will be denoted as $k_{r,i}$. This factor is a generalisation of the factor introduced by SUGISHITA [3].

Flow field distortion effect The direction of the velocity vectors of the flow field is altered in the neighbourhood of the transducers. The effect is strongly dependent on the transducer geometry. Usually the distortion is such that the measured mean path velocities will be *lower* in magnitude. This correction factor for the i-th path will be denoted as $k_{f,i}$

The overall protrusion coefficient $k_{prot,i}$ of path i for a given transducer pair is then approximated by the product

$$k_{prot,i} = k_{f,i} k_{r,i} \tag{2}$$

[1] For further reading on quadrature errors, see [2]

In many situations the two effects are such that they partly compensate each another. The international code of ASME-PTC 18 [4] reports of combined negative errors between 0.05 % (1m path lengths) and 0.35 % (5m path lengths) for certain tranducers. The following two sections will discuss these effects in more detail.

2 Reduced Path Length Effect

It is desired to have a mathematical description of an acoustic path in $\mathbb{R}^3$. This description allows the calculation of the actual path length, as well as the orientation of the transducer face. The following derives such a description.

2.1 General Problem Formulation

This section gives a brief introduction to the notation used for the following derivation. Let $\boldsymbol{r}_{AB} \in \mathbb{R}^3$ be a vector in three dimensional EUCLIDEAN space, which is directed from point A to point B. Any vector space must obey addition and scalar multiplication, in particular, $\boldsymbol{r}_{AC} = \boldsymbol{r}_{AB} + \boldsymbol{r}_{BC}$. In order to perform the addition, some frame of reference (FOR) is necessary. There is an unlimited number of possible choices to define a FOR. In the following, the I frame is an *inertial* FOR and $\mathcal{O}$ is its origin. The unit vectors of I are $\boldsymbol{e}_x^I$, $\boldsymbol{e}_y^I$ and $\boldsymbol{e}_z^I$ for the x, y and z directions, respectively. Therefore, ${}_I\boldsymbol{r}_{AB}$ is the above vector described in the inertial FOR I with components $(x\ y\ z)^T$.

Suppose we have a transducer which is mounted from outside by drilling a hole through the conduit wall. Such transducer has a rotational degree of freedom about its principal axis. This DOF will be referred to as γ in the following. Additionaly, the normal to the face of the transducer that radiates the acoustic signal may be aligned at an angle δ to the principal axis of the transducer. For an illustration, refer to Figure 1b. In addition to the above features, the transducer may be mounted at any angle α on the circumference of the conduit wall. The main concern in this section is to derive expressions for the coordinates of vector $\boldsymbol{r}_{TP}$ in a suitable coordinate system. As can be seen from Figure 1a, $\boldsymbol{r}_{TP}$ points in the direction of the acoustic path and $\|\boldsymbol{r}_{TP}\|$ is its length. The idea to determine $\boldsymbol{r}_{TP}$ is to find its intersecting point P on the conduit surface. Ideally, the acoustic path is incident *normal* to the transducer face. Hence, the most suitable coordinate system in which $\boldsymbol{r}_{TP}$ should be described is the one with two axes in the plane of the transducer face and the third axis is normal to the other two.

As already introduced above, we wish to find $\boldsymbol{r}_{TP}$, which is the vector pointing from the transducer face T to the intersecting point, P, on the conduit surface. As depicted in Figure 1a, the relation

$$\boldsymbol{r}_{TP} = \boldsymbol{r}_{T\mathcal{O}} + \boldsymbol{r}_{\mathcal{O}P} \tag{3}$$

must hold.

Vector ${}_C\boldsymbol{r}_{TP}$ is the vector of Eq. (3) represented in FOR C. In that coordinate system, ${}_C\boldsymbol{r}_{TP}$ is equal to a straight line with direction along $-\boldsymbol{e}_y^C$, the minus sign arises from the definition of FOR C (see Figure 1b). Equating the two quantities yields the system

$$\begin{pmatrix} h\sin\delta + x\cos\gamma\cos\delta + R(c_{11}\cos\beta + c_{12}\sin\beta - \sin\delta) \\ h\cos\delta - x\cos\gamma\sin\delta + R(c_{21}\cos\beta + c_{22}\sin\beta - \cos\delta) \\ x\tan\gamma - R(\sin\alpha\cos\beta - \cos\alpha\sin\beta) \end{pmatrix} = \begin{pmatrix} 0 \\ -t \\ 0 \end{pmatrix} \tag{4}$$

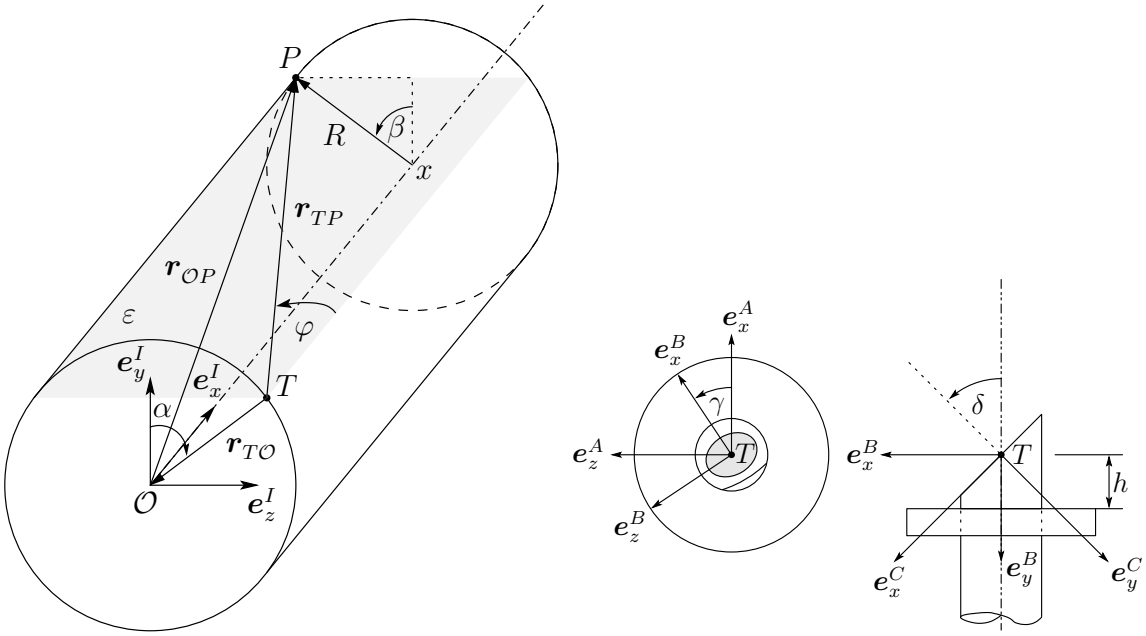

(a) Orientation in $\mathbb{R}^3$ of an acoustic path in a circular conduit.

(b) Orientation of the transducer in $\mathbb{R}^3$.

Figure 1 Illustrations to help understand the involved coordinate transformations. Subfigure (a) shows the orientation in $\mathbb{R}^3$ of an acoustic path inside a circular conduit. The path must lie in the acoustic plane (elevation plane ε) which is parallel to the principal axis of the conduit. The orientation of the transducer is shown in figure (b). The transformations $\mathcal{A}_{BA}$ and $\mathcal{A}_{CB}$, which are determined by the angles γ and δ, are also illustrated.

with constants

$$c_{11} = \sin\delta\cos\alpha + \sin\gamma\cos\delta\sin\alpha \tag{5}$$

$$c_{12} = \sin\delta\sin\alpha - \sin\gamma\cos\delta\cos\alpha \tag{6}$$

$$c_{21} = \cos\delta\cos\alpha - \sin\gamma\sin\delta\sin\alpha \tag{7}$$

$$c_{22} = \cos\delta\sin\alpha + \sin\gamma\sin\delta\cos\alpha \tag{8}$$

A derivation of this system is given in Appendix A.

The system of Eq. (4) can be used to calculate an arbitrary acoustic path in $\mathbb{R}^3$. However, the system of equations introduces five unknowns, of which three are related to finding the intersecting point P. Therefore, two unknows must be eliminated by introducing two constraints.

It is desired for an ADM application that the acoustic paths are *parallel* to the principal axis of the conduit (they lie in the ε-plane) and that the paths are aligned at an angle φ in the ε-plane, see Figure 2. This information is sufficient to eliminate the two unknowns γ and δ in a first step and then solve for the intersection point P, i.e., x, β and t, in a second step.

2.2 Path Constraints for Determination of γ and δ

In this section we derive two relations by introducing two constraints. This will reduce the unknows in system of Eq. (4) to three and, hence, can be solved with three equations. These constraints are:

i.) The acoustic path must lie in the ε-plane, which is *parallel* to the principal axis of the conduit. Because $\boldsymbol{e}_x^I$ is *collinear* with the principal axis, the two points T and P can *only* lie in ε if

$$\|_B \boldsymbol{r}_{T\mathcal{O}}\| = R \tag{9}$$

Eq. (9) can only hold if $h = 0$, i.e., the point T on the transducer face is on the conduit surface. Due to symmetry

$$h = 0 \implies \beta = -\alpha \tag{10}$$

ii.) The acoustic path is aligned at an angle φ in the ε-plane. If the constraint in i.) holds, then the length of the acoustic path and the x-coordinate for the intersecting point P are given by, respectively

$$L_0 = \frac{2R'}{\sin\varphi} = 2R\frac{\sin\alpha}{\sin\varphi} \tag{11}$$

$$x_0 = L_0\cos\varphi = 2R\frac{\sin\alpha}{\tan\varphi} \tag{12}$$

The subscript 0 indicates that $h = 0$. See Figure 2 for a visualization. Since t is the length of the acoustic path, it follows that $t = L_0$.

Given these two constraints, the system of Eq. (4) reduces to

$$\begin{pmatrix} \cos\varphi\cos\gamma\cos\delta - \sin\varphi\sin\alpha\sin\delta + \sin\varphi\cos\alpha\sin\gamma\cos\delta \\ \cos\varphi\cos\gamma\sin\delta + \sin\varphi\sin\alpha\cos\delta + \sin\varphi\cos\alpha\sin\gamma\sin\delta \\ \tan\gamma - \tan\varphi\cos\alpha \end{pmatrix} = \begin{pmatrix} 0 \\ 1 \\ 0 \end{pmatrix} \tag{13}$$

The third equation of the above system is decoupled and can be used to explicitly calculate γ with given φ and α, i.e.,

$$\tan\gamma = \tan\varphi\cos\alpha \tag{14}$$

The angle α defines the elevation of the ε-plane. An explicit relation for δ can be obtained from the first equation of the set in Eq. (13), i.e.,

$$\tan\delta = \frac{\cos\gamma}{\tan\varphi\sin\alpha}\left(1 + \tan\varphi\cos\alpha\tan\gamma\right) \tag{15}$$

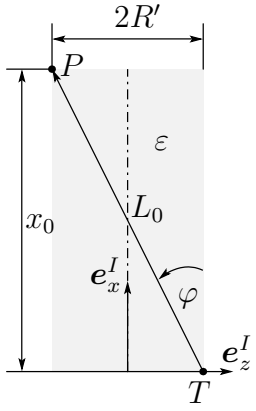

Figure 2 Configurations in the elevation plane ε. Figure shows a configuration from wall to wall, where T and P do not protrude into the flow field.

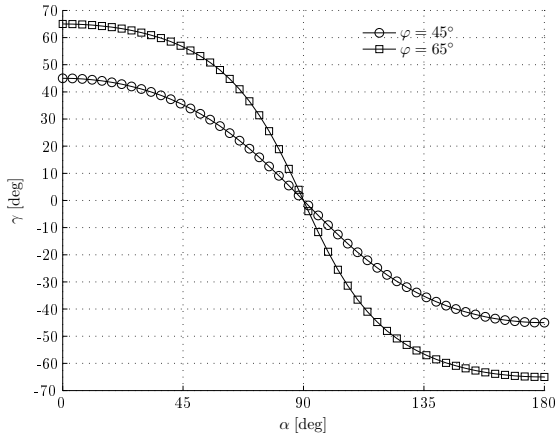

(a) Rotational degree of freedom γ about the principal axis of the transducer as a function of the angular location α of the end points of the acoustic path.

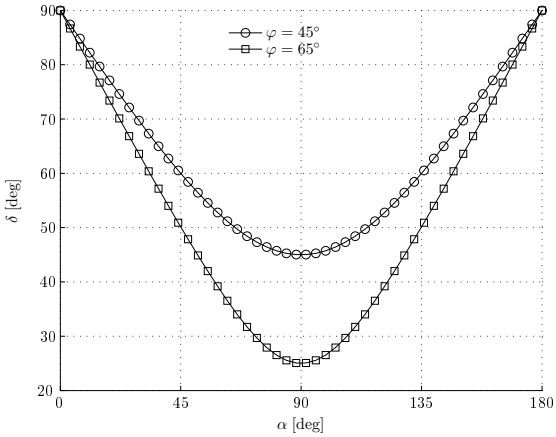

(b) Inclination δ of the transducer face as a function of the angular location α of the end points of the acoustic path.

Figure 3 Evaluation of γ and δ on the interval $0 \leq \alpha \leq \pi$, such that the acoustic path lies in the plane ε of Figure 1a. These angles define the coordinate transformations $\mathcal{A}_{BA}$ and $\mathcal{A}_{CB}$.

The last of the three equations in Eq. (13) can be used as a check.

Given Eq. (14) and (15), one can first calculate γ and then δ. The system of Eq. (4) then reduces to the three unknowns x, β and t. γ and δ are illustrated in Figure 3 for $\varphi = 45°$ and $\varphi = 65°$, for positions of the ε-plane ranging from $0 \leq \alpha \leq \pi$. Note that these figures are *only* valid if the path is contained in ε. The very general approach to calculate γ and δ without the constraints used for an ADM calculation is given in Appendix B.

2.3 Determination of Protrusion Lengths

Assuming the radius R, point T, γ and δ are known, then the system of three equations given in Eq. (4) can be solved for the unknowns x, β and t, that is point P, where

x: The x-coordinate of point P in FOR I.

β: Angle on the conduit surface between point P and $\boldsymbol{e}_y^I$ with intersection at $\mathcal{O}$. The sign of β obeys the right hand rule along $\boldsymbol{e}_x^I$.

t: Length of the straight line between point T and P.

The procedure to arrive at P is to first determine γ and δ with Eq. (14) and Eq. (15), if the path angle φ is known. Alternatively, γ and δ can be determined by Eq. (38) and Eq. (39) if two points on the acoustic path are known, e.g., from measurements. After determination of γ and δ, the system of Eq. (4) can be solved with a suitable numerical algorithm.

The following is a post-calculation of the acoustic paths with length L_i and the associated protrusion length L_T for a specific ADM installation. Due to installation errors, the mounted transducers may violate the assumption that they must lie in the ε-plane slightly. Therefore, we follow two approaches. First we calculate the path lengths exactly. A second calculation uses a projection of the acoustic path onto the ε-plane and then follows

Path	Exact				Projection				
	L_i [mm]	$L_{T,1}$ [mm]	$L_{T,2}$ [mm]	$L_{T,1}+L_{T,2}$ [mm]	L_i [mm]	$L_{T,1}$ [mm]	$L_{T,2}$ [mm]	$L_{T,1}+L_{T,2}$ [mm]	Δy_i [mm]
1	4854.53	33.20	29.60	62.80	4854.53	33.56	29.24	62.80	0.46
2	7956.70	11.75	16.11	27.86	7956.70	12.92	14.94	27.86	6.48
3	7941.68	22.43	26.47	48.90	7941.68	20.93	27.97	48.91	8.37
4	4834.36	51.99	61.18	113.17	4834.36	56.06	57.11	113.17	5.25

Table 1 Exact and approximate calculation of the acoustic path length (from transducer face to transducer face) and the protrusion length $L_{T,i}$ (from transducer face to conduit wall). The approximate calculation is based on a projection of the two measured points onto a plane which is located at the arithmetic mean of the y-coordinates of the two points. The value Δy_i is the absolute deviation in the y-direction relative to the two points.

§ 2.2. The projection therefore is an approximation to the exact calculation. The results of the calculations for four paths are summarized in Table 1. The table illustrates, that the projection onto a plane is a reasonable approximation. However, note that the individual protrusion lengths, $L_{T,i}$, for either transducer, does vary rather significantly for some paths. However, the effect is compensated when looking at the *sum* of the two protrusion lengths of an acoustic path.

2.4 Determination of $k_{r,i}$

The correction we wish to find must satisfy the relation

$$\bar{v}_{x,i} = k_{r,i}\hat{v}_{x,i} \tag{16}$$

where $\bar{v}_{x,i}$ is the mean velocity in the main flow direction along the acoustic path i *without any effects of protrusion* and $\hat{v}_{x,i}$ is the analogon *with protrusion*. Due to the reduced path length effect we have $\bar{v}_{x,i} < \hat{v}_{x,i}$ and therefore it follows $k_{r,i} < 1$, since we wish to correct the measured velocity in such a way that we get the velocity as if there was no protrusion effects. Hence, the correction factor $k_{r,i}$ is defined by the ratio of mean velocities along the acoustic path i.

To find $k_{r,i}$, we need to find the mean velocities along the acoustic path. In general, any steady velocity profile $v_x = v_x(\boldsymbol{r})$ is possible, where the vector $\boldsymbol{r} = (x\, y\, z)^T$ contains the spatial coordinates. v_x may be a mathematical model or a set of data for which interpolation can be used to find the value at x, y and z. The mean velocity along some path with length L_i is then computed by

$$\bar{v}_{x,i} = \frac{1}{L_i}\int_{c}^{c+L_i} v_x(\tau)\mathrm{d}\tau \tag{17}$$

with some constant c. Because we integrate along a path in $\mathbb{R}^3$, the velocity profile must be parameterized with some parameter τ.

If two points $T, P \in \mathbb{R}^3$ are known to lie on a path, then the coordinates of any point on that path are given by the relation

$$\boldsymbol{r}(\tau) = \boldsymbol{r}_{\mathcal{O}T} + \frac{\tau}{\|\boldsymbol{r}_{\mathcal{O}P} - \boldsymbol{r}_{\mathcal{O}T}\|}(\boldsymbol{r}_{\mathcal{O}P} - \boldsymbol{r}_{\mathcal{O}T}) \tag{18}$$

in FOR I. Assuming point T is on the trancducer face, as shown in Figure 1b, the limits for integration are readily determined. Determining L_i, $L_{T,1}$ and $L_{T,2}$, as discussed in § 2.3, the correction factor $k_{r,i}$ can be calculated by

$$k_{r,i} = \frac{L_i}{L_i + L_{T,1} + L_{T,2}} \frac{\int_{-L_{T,1}}^{L_i+L_{T,2}} v_x(\tau)\,\mathrm{d}\tau}{\int_0^{L_i} v_x(\tau)\,\mathrm{d}\tau} \tag{19}$$

Note that due to the integration along the parameterized acoustic path, Eq. (19) also introduces an implicit correction for erroneously mounted transducers, since $L_{T,1}$ and $L_{T,2}$ explicitly appear in the limits of the integrals. This "hidden" error vanishes if the path from transducer face to transducer face, defined by points T and P, *is exactly centered about the principal axis of the conduit*. Also, it is important to realize, that with the above introduced definitions, the lengths $L_{T,1}$ and $L_{T,2}$ *are positive if the points T and P lie inside the conduit and negative if the corresponding point lies outside the conduit*. Otherwise the limits of integration will be wrong.

Figure 4 shows the correction factors $k_{r,i}$ according to Eq. (19) for a 9-path ADM installation at OWICS positions (full lines) and GAUSS-JACOBI positions (dashed lines). The corrections depend on how far the transducer protrudes into the conduit. Therefore, the fraction of protrusion, p_f, is defined by

$$p_f = \frac{h}{R} \tag{20}$$

The computations shown in Figure 4 use the following model for the velocity profile

$$v_x = v_{\max}\left(1 - \frac{y^2 + z^2}{R^2}\right)^{\zeta} \tag{21}$$

The coefficients $v_{\max}$ and ζ are determined such that the flow has a REYNOLDS number of 5×10^6 (Figure 4a) and 5×10^7 (Figure 4b). Note that the model velocity of Eq. (21) has three important properties

1. $\partial v_x/\partial x = 0$, i.e., the velocity profile is *fully developed*.
2. The velocity profile has *rotational symmetry*.
3. The area flow function is of the same form as Eq. (21). However, the factor $v_{\max}$ will be different and the shape of the curvature is given by the exponent κ instead of ζ. The two exponents are related by $\kappa = \zeta + \frac{1}{2}$.

If a velocity profile shows the first two characteristics, the correction factors $k_{r,i}$ *will never depend on the path angle φ*.

As can be seen from Figure 4, if the REYNOLDS number of the flow *increases*, the reduced path length effect *decreases*. At higher REYNOLDS numbers, the shape of the velocity profile tends towards a rectangular profile and reaches the GAUSS-JACOBI velocity profile at $\kappa = 0.5$ in the limit. In fact, if a rectangular velocity profile is used, the reduced path length effect vanishes and the correction factors on each path would be unity. That is, high REYNOLDS numbers are preferable in order to minimize the reduced path length effect.

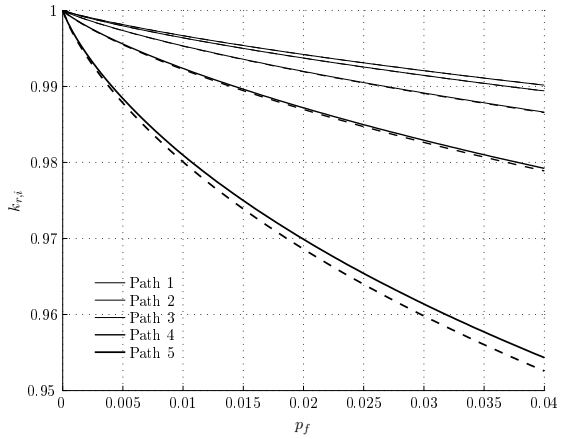

(a) $Re = 5 \times 10^6$, $\zeta = 0.0935$

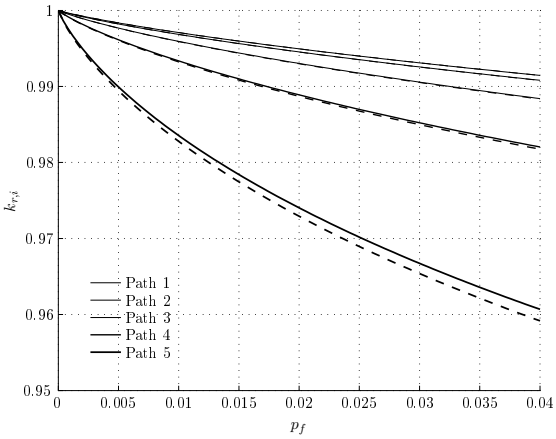

(b) $Re = 5 \times 10^7$, $\zeta = 0.0796$

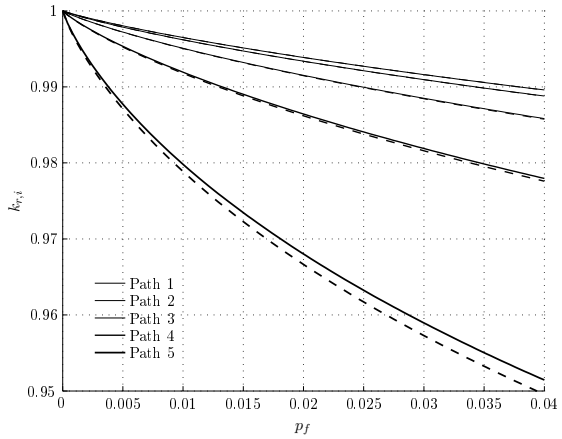

(c) Standard OWICS, $\zeta = 0.1$. Note that the second and fourth path are used for the 4-path ADM (*only true for* GAUSS-JACOBI *positions*).

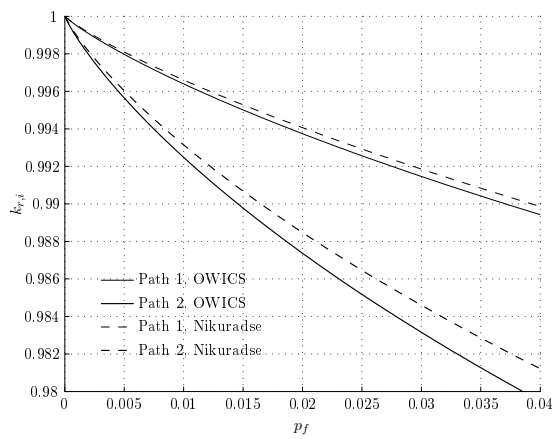

(d) Comaprison of OWICS velocity model and the NIKURADES $1/n$-power law on a 4-path ADM. The positions of the paths correspond to the OWICS model.

Figure 4 Figure 4a, 4b and 4c show the correction factors $k_{r,i}$ for a 9-path ADM for a velocity model given in Eq. (21). The first two use an adaptive approach to determine ζ of the velocity profile with the given REYNOLDS numbers. The third figure uses standard OWICS, i.e., $\zeta = 0.1$. Full lines represent paths at OWICS positions, whereas the dashed lines represent paths located at GAUSS-JACOBI positions. Path 1 is the *inner most* path and Path 5 is the *outer most* path. Note that the different path locations get more relevant on paths that are located further away from the center axis of the conduit. Also, the correction factors tend towards one, the higher the turbulent energy of the flow. Figure 4d compares the OWICS model with the power law model by NIKURADSE. The paths are located at OWICS positions. The figure shows that the OWICS model needs a slightly stronger correction than the power law model.

3 Flow Field Distortion Effect

3.1 Transducer Arrangement

Depending on the geometry of the transducer and its orientation inside the conduit, two different cases can be distinguished as is illustrated in Figure 5.

Figure 5a: This is the case when the transducer faces *upstream*, i.e., against the main direction of flow. It is assumed that the measurement membrane of the transducer is

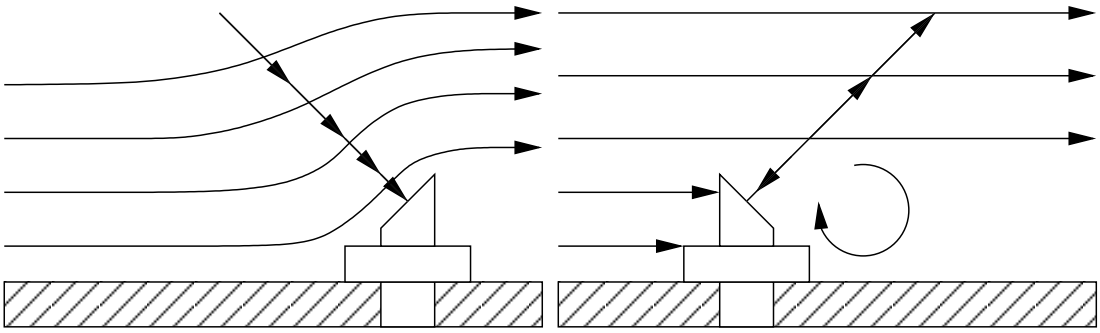

(a) Streamlined flow regime in the measurement zone.

(b) Separated flow regime in the measurement zone.

Figure 5 The present figure illustrates the two different cases which can be distinguished related to protrusion for a drilled in mounted transducer. Figure (a) shows the case where the measurement face of the transducer points *upstream*. Streamlines follow the outline of the measurement face. *The main characteristic of that case is that there is no flow separation in the measurement area.* Figure (b) illustrates the second case where the transducer measurement face points *downstream*. *The characteristic here is that there is a region of separated flow located in the zone of measurement.*

aligned at an angle δ along its principal axis. Further, the streamlines of the flow follow the contour of the transducer *without* separating from the surface. Recall that the velocity induced by the flow field onto the acoustic path is the projection of the velocity vector in a frame of reference that is aligned with the acoustic path. For further reading on how the transit time method works, see, e.g., §1.1 of [6]. Due to the protruding transducer, the streamlines are redirected in a region of flow close to it. The realignment of the streamlines reduces the angle between the velocity vector and the normal axis of the frame of reference aligned with the acoustic path. A reduction of the angle results in a projected velocity that is *smaller* than the projected velocity without protrusion. In the worst case, the velocity vector is normal to the acoustic path and the projected velocity is zero. Therefore, the measured mean velocity will be lower in magnitude. Note that the *sign* of the projected velocities *will not change*.

Figure 5b: This is the case when the transducer faces *downstream*, i.e., along the direction of flow. The fluid flow is interrupted by the transducer and flow separation is likely to occur in the zone of measurement. The effect is the same as in Figure 5a, with the exception that the sign of the projected velocity may change due to the secondary flow appearing in that region. The sign inversion allows a locally stronger influence of protrusion, hence, the overall effect can be larger for this case (Figure 5b) than for the case depicted in Figure 5a.

3.2 Transducer Types

Several types of transducers exists depending on the installation requirements. Typically the size of the transducers vary with the emitting frequency, with getting larger by decreasing the frequency. The larger impact on the protrusion effect has however the way the transducer is mounted, drilled in or mounted from the inside. The following two pictures show each an example of a drilled in (Figure 6b) and mounted from the inside (Figure 6a) transducer.

(a) Mounted from the inside, types MFATB2.001 and MFATB05

(b) Mounted by drilling a hole through the conduit wall, type MFATAxx

Figure 6 Two commonly used transducer types. Figure 6b shows a transducer that is mounted by drilling a hole through the conduit wall. Figure 6a shows a transducer type that is entirely mounted from the inside of the conduit.

3.3 Simulation

As the flow around the transducer locations is of particular interest in this study, the simulation domain was chosen such that these circumstances could be met. Two regions were selected, one for a centre path location (α=90°) and one for an outermost path (α=18°) of an 18 path (two 9 paths crossed) confuguration. The path angle φ is chosen as 45°. It is assumed that the protrusion effect for paths with positions with angles between 18° and 90° lies between the two extreme considered situations. For each of the two regions a sector of 45° and of a depth of half of the radius. This allows to simulate half the path length for the outermost path and a quarter length for the centre path. The flow field is assumed to be symmetrical with respect to the centre line of the conduit; therefore the simulated parts of the flow field could be used for certain transducers for its influence on the upstream as well on the downstream mounted cases. As the length of the largest inside mounted transducer is around 25cm, the length of the simulated section of the the conduit was chosen as 5m in order to achieve a sufficiently well modelled region around the transducer, /ie, a fully developed velocity profile. For the boundary conditions of inlet and outlet flows and walls the following was chosen:

- Diameter of 5m and velocities of 1m/s and 10m/s leading to Reynolds numbers of 5×10^6 and 5×10^7.
- Periodic boundary conditions between inlet and outlet.
- No slip boundary conditions at the wall.

The mesh for the simulation has been chosen as follows:

- Structured grid with 376000 elements for the far field.
- Unstructured grid with 126000 elements for the near field around the transducer. This discretization leads to certain quantization effects as can can be seen in Figure 8. A finer resolution of the velocities in the boundary layer would require a higher number of elements. This approach will have to be taken in order to be more confident on the results.

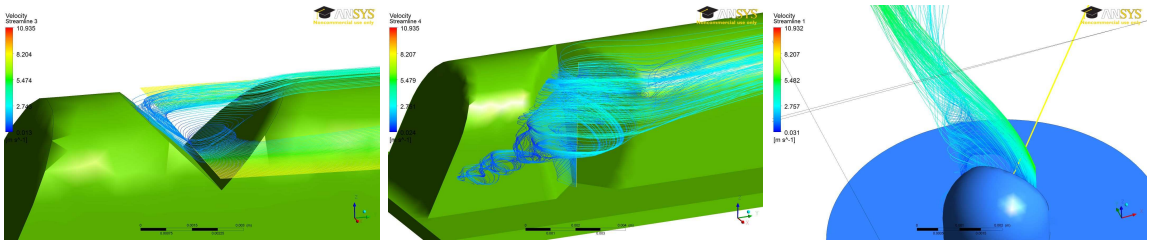

(a) $\alpha = 90°$ **(b)** $\alpha = 18°$ **(c)** $\alpha = 18°$

Figure 7 Illustration of the rotational velocity field in the vicinity of the transducer face. This flow is induced by the physical presence of the transducer. The associated error that occurs by this effect is corrected with the factor $k_{f,i}$.

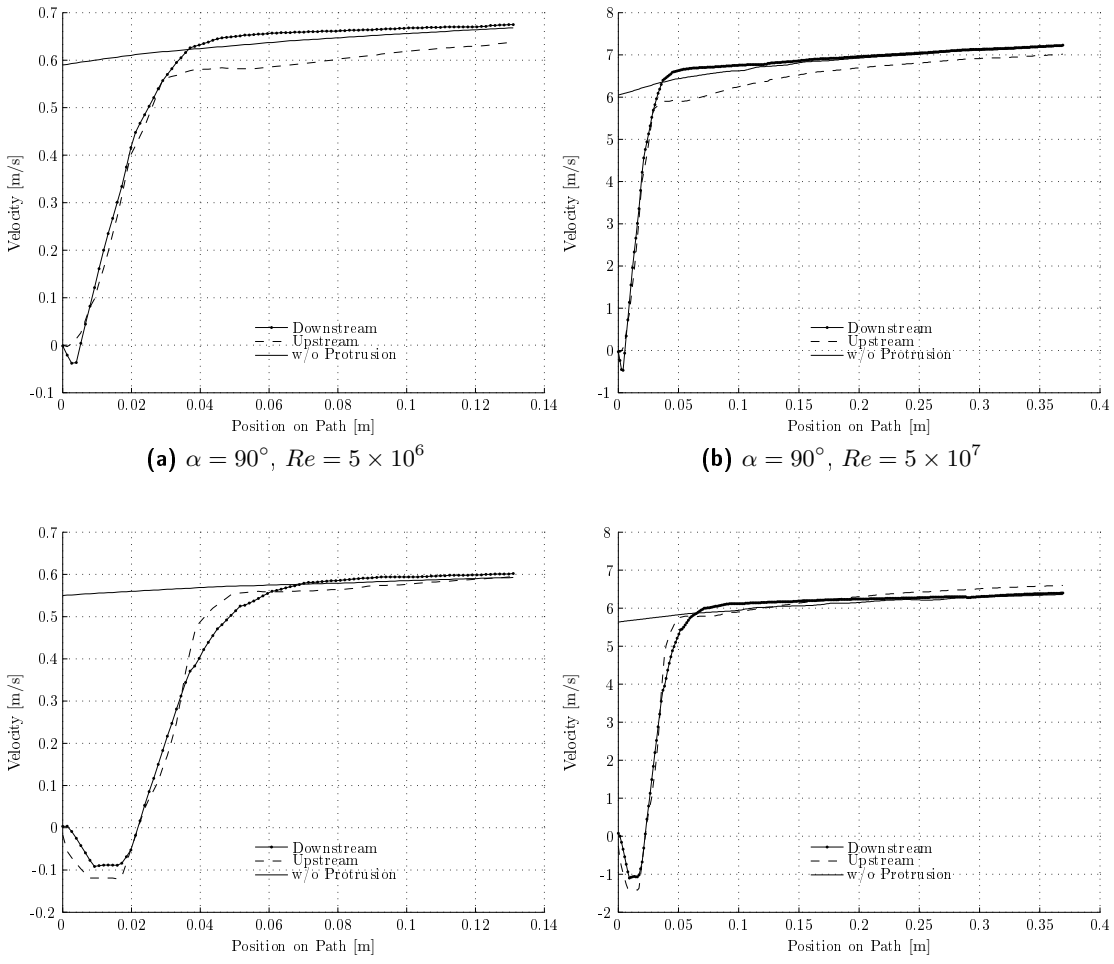

(a) $\alpha = 90°$, $Re = 5 \times 10^6$ **(b)** $\alpha = 90°$, $Re = 5 \times 10^7$

(c) $\alpha = 18°$, $Re = 5 \times 10^6$ **(d)** $\alpha = 18°$, $Re = 5 \times 10^7$

Figure 8 Velocities along an acoustic path in the vicinity of the transducer face. The highly rotational flow field (see Figure 7) causes the velocity to change direction. The change in direction results in measured mean velocities that are too low and must be corrected with a factor $k_{f,i} > 1$. The plots correspond to the MFATB05 transducer types.

Overall simulations have been carried out for a combinaton of 2 path positions, 2 flow conditions and 3 transducer types (two inside mounted, one drilled in). The smaller inside

mounted sensor MFATB2.001 and the drilled in sensor MFATAxx were simulated for the outermost path (α=18°) only, therefore 8 cases have been considered. Figure 7a and Figure 7b show two cases of an inside mounted sensor at two different positions. It is clearly visible, that a vortex inducing backflow is created in the V-notch where the sensor pills are located. This leads to velocity distributions along the acoustic path as shown in Figure 8. It is interesting to notice that in the upstream as well as in the downstream case a backflow can be observed. This fact is much dependent on the transducer design. VOSER presented results with transducers from a different manufacturer where the backflow could only be observed for the upstream case [5]. Figure 7c shows a simulation result for the drilled in sensor. It can be seen that the disturbed flow field affects the path line only for a short distance of the path near the sensor. The greatest part of the distortion is deflected away from the acoustic path. If the protruding height h of the transducers are small, its influences are also small. Further simulation results can be found in [1].

4 Results

4.1 Determination of correction factors $k_{r,i}$ and $k_{f,i}$

The simulations of § 3 and the results of § 2 allow to determine the correction factors $k_{r,i}$ and $k_{f,i}$ in different ways. The obtained results hold strictly spoken only for the considered case of a 5m diameter pipe and a path angle φ of 45° [2]. The path index i is omitted in the following as it is identified from the angle α. The listed averaged velocities were extracted from the simulations:

- $\hat{v}_x^{meas}$: This is the *measured* velocity of an ADM installation from transducer face to transducer face. It contains *both* effects of protrusion, i.e., reduced path length effect *and* flow field distortion effect.
- $\hat{v}_x$: This is the velocity measured from transducer face to transducer face, where the velocity field contains no distortion induced by the presence of a transducer. The notation for this mean velocity has already been introduced in § 2.4.
- $\bar{v}_x$: This is the mean velocity from conduit wall to conduit wall without any possible distortions in the velocity field induced by the presence of a transducer. The notation for this velocity has also already been discussed in § 2.4.

From these quantities the following ratios can be obtained:

- the overall measurement error $\epsilon = \hat{v}_x^{meas.}/\bar{v}_x$
- the flow field distortion correction factor $k_f = \hat{v}_x/\hat{v}_x^{meas.}$
- the reduced path length corretion factor $k_r = \bar{v}_x/\hat{v}_x$

The results of Table 2 lead to a number of conclusions:

- Different REYNOLDS numbers (different velocities) for the same case have only a very small influence. The flow distortion around the tranduscers change only slightly.

[2] Note that *if the velocity profile is fully developed and has rotational symmetry*, then the path angle φ has only an effect on $k_{f,i}$ but not $k_{r,i}$.

- The difference in path lengths between center and outermost paths is reflected in a in-/decrease in the influence of the flow field distortion. The formula for the path length $L_{W_i} = L_0$ for the case of no protrusion is given by Eq. (11). It follows that the outermost path is reduced by a factor of ≈ 0.3 for a path angle of $\varphi = 45°$. The flow field distortion correction k_f is decreased from ≈ 1.026 (case MFATB05, α=18°) to ≈ 1.005 (case MFATB05, α=90°), that means the error is increased by a factor of ≈ 5 while the path length is shorten by factor of 3.33. Therefore one might conclude that the influence from center to outermost paths grows more than proportional if the path length difference is eliminated. This might be because the outer most path remains for a longer distance close to the boundary layer.

- The flow distortion effect leads always to an underestimation of the averaged velocity, which is reflected in a k_f factor greater than one.

- If the α=18° cases are compared, then one concludes, as can be expected, that the smaller the transducer is, the smaller is its flow distortion effect, which means k_f gets closer to one. Simulations for the other angles have to be carried out to confirm this result. A similar trend can be observed for the reduced path length correction factor k_r^{mod} derived from the model correction curves of Figure 4.

- The overall error ϵ is except for two cases greater than one and in absolute terms always smaller than 1%. For the listed α=90° case there is a slight overestimation of 0.15% (mean value) compared to the true value. In this case a correction with the model correction factor k_r^{mod} for compensating the reduced path length effect gives not a better result (last column).

- To get the overall influence for a multipath configuration, each path has to be treated separately and weighted according to the flow integration formula. For a 18-path application one has to cope with the wide spread of path lengths: the inner paths are less affected from the effect than the outer paths.

In the error analysis of an ADM measurement system an overall protrusion error of less than 0.1% does no more contribute significantly to the overall error and can therefore be neglected. As this could be more or less verified only for the α=90° cases (MFATB05) it remains open how small the effect will be for the other transducers for other than the α=18° positions.

4.2 Generalization for correction coefficient

All simulations have been done so far for a 5m conduit. It is possible to extrapolate the results for each transducer and positions to smaller and larger diameter under the assumption that the flow distortion around the transducer do not change. This extrapolation is shown in Figure 9 for the MFATB05 α=90° cases (two REYNOLDS numbers). The compensating effect of the two influences can be seen. For small values of r, the spread between the two curves widens while for values of r greater than $\approx$ 4m both effects are very close to one.

Transducer Type	Re [−]	$\hat{v}_x^{meas.}$ [a] [m/s]	$\hat{v}_x$ [b] [m/s]	$\bar{v}_x$ [c] [m/s]	$\hat{v}_x^{meas.}/\bar{v}_x$ [−]	k_f [d] [−]	k_r [e] [−]	$k_r^{mod.}$ [f] [−]	$k_f k_r$ [−]	$k_f k_r^{mod.}$ [−]
MFATB05	5×10^6	0.6356	0.6514	0.6358	0.9997	1.0250	0.9761	0.9698	1.0005	0.9941
$\alpha = 18°$	5×10^7	6.4059	6.5800	6.4487	0.9934	1.0270	0.9801	0.9739	1.0065	1.0002
MFATB05	5×10^6	0.7458	0.7482	0.7441	1.0024	1.0030	0.9945	0.9945	0.9975	0.9975
$\alpha = 90°$	5×10^7	7.2912	7.3469	7.2867	1.0006	1.0076	0.9918	0.9952	0.9994	1.0028
MFATB2.001	5×10^6	0.6327	0.6419	0.6268	1.0094	1.0150	0.9765	0.9755	0.9911	0.9901
$\alpha = 18°$	5×10^7	6.4142	6.5031	6.3608	1.0084	1.0140	0.9781	0.9788	0.9918	0.9925
MFATAxx	5×10^6	0.6187	0.6265	0.6171	1.0026	1.0130	0.9850	0.9848	0.9978	0.9976
$\alpha = 18°$	5×10^7	6.2777	6.3505	6.2604	1.0028	1.0120	0.9858	0.9868	0.9976	0.9986

[a] This is the *measured* velocity of an ADM installation from transducer face to transducer face. It contains *both* effects of protrusion, i.e., reduced path length effect *and* flow field distortion effect.

[b] This is the velocity measured from transducer face to transducer face, where the velocity field contains no distortion induced by the presence of a transducer. The notation for this mean velocity has already been introduced in § 2.4.

[c] This is the mean velocity from conduit wall to conduit wall without any possible distortions in the velocity field induced by the presence of a transducer. The notation for this velocity has also already been discussed in § 2.4.

[d] Flow field distortion correction factor, $k_f = \hat{v}_x/\hat{v}_x^{meas.}$.

[e] Reduced path length corretion factor, $k_r = \bar{v}_x/\hat{v}_x$. The value for this factor is determined from the simulation.

[f] The same correction factor as in item e, but determined with the model velocity profile of Eq. (21).

Table 2 Summary of the simulation results for the MFATB2.001, MFATB05 and MFATAxx transducers. The positions corresponding to α are GAUSS-JACOBI positions. The modeled correction factors for the reduced path length effect, $k_r^{mod.}$, are given by the dashed lines of Figure 4a and 4b for the two different REYNOLDS numbers.

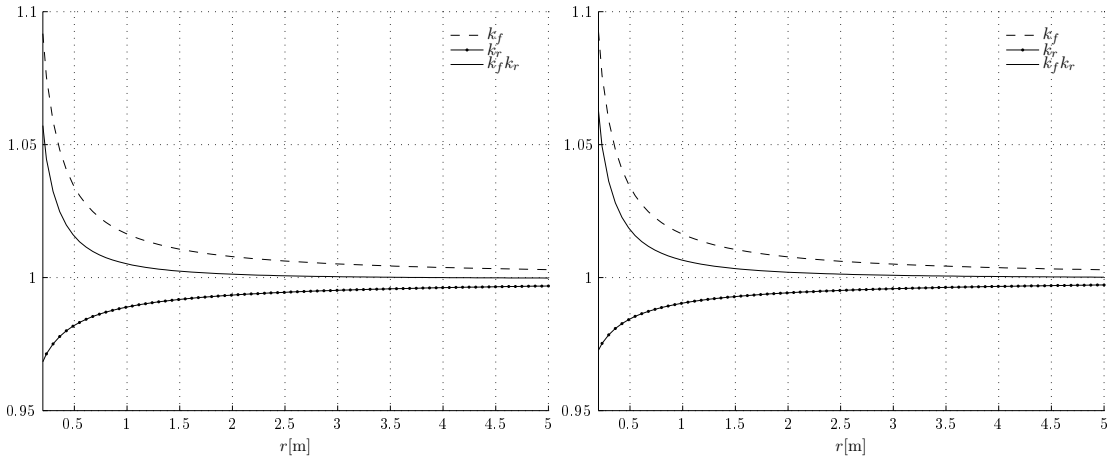

(a) $\alpha = 90°$, $Re = 5 \times 10^6$ **(b)** $\alpha = 90°$, $Re = 5 \times 10^7$

Figure 9 Distribution of the correction factors k_f and k_r dependent on the radius r for the MFATB05 transducer. The product of the two correction factors is also shown.

5 Conclusions

In this study the two influences, the reduced path length effect and the flow field distortion effect has been studied. From the work done so far the following conclusions can be drawn:

- For the reduced path length effect, correction curves could be derived which depends on the protrusion depth $p_f = h/R$, the assumed velocity profile and the path position. These curves are a generalization of the results of the correction given in [3]. Note that the reduced path length correction is an isolated *geometrical* problem.
- The simulation results confirm the trend that for large conduits the influence of the flow field distortion effect gets smaller as the absolute distortion remains the same. The dependence on the REYNOLDS number for the cases considered is small.
- In order to quantify the flow field distortion effect more precisely, the discretization chosen for the simulations has to be refined. Also it will be necessary to widen the simulations for each transducer type to all the important path positions (18°, 36°, 45°, 54°, 72°, 90°). The cases chosen in this study were not conclusive enough.
- In addition, the influence of the radius of the conduit on the flow field correction factor $k_{f,i}$, as extrapolated in Figure 9, should be verified by further simulations too.
- The considerations in § 2 provides a general mean for the calculation of an acoustic path contained in a circular conduit. Such path has an origin point given by T and two additional degrees of freedom, i.e., rotation about the angles γ and δ, as defined in Figure 1b.

References

[1] F. DESCHWANDEN, *Protrusioneffekt von Sensoren bei akustischen Durchflussmessungen.* Bachelor Thesis, June 2012.

[2] P. GRUBER, T. STAUBLI, T. TRESCH, AND F. WERMELINGER, *Optimization of the ADM by adaptive weighting for the gaussian quadrature integration*, in Roorkee 2010, IGHEM, 2010. `http://www.ighem.org/`.

[3] K. SUGISHITA, A. SAKURAI, H. TANAKA, AND T. SUZUKI, *Evaluation of error of acoustic method and its verification by comparative field tests*, in Montreal 1996, IGHEM, 1996. `http://www.ighem.org/`.

[4] VARIOUS, *Hydraulic Turbines and Pump-Turbines: ASME PTC 18-2011: Performance Test Codes*, 2011.

[5] A. VOSER, *Analyse und Fehleroptimierung der mehrpfadigen akustischen Durchflussmessung in Wasserkraftanlagen*, PhD thesis, ETH Zürich, 1999.

[6] F. WERMELINGER, *Optimization of acoustic discharge measurements with regard to protrusion effects and transient velocity fields.* Bachelor Thesis, June 2010.

A Coordinate Transformations

It is most convenient to represent $\boldsymbol{r}_{TP}$ of Eq. (3) in a FOR C that has one axis normal to the transducer face. In order to get from I to C, three rotations (i.e., coordinate transformations) must be performed. These are

i.) Rotation of α in the *positive* direction along $\boldsymbol{e}_x^I = \boldsymbol{e}_x^A$. This rotation allows for arbitrary positioning of the transducer on the circumference of the conduit, relative to the position of the acoustic plane ε. The transformation is represented by the matrix $\mathcal{A}_{AI} \in \mathbb{R}^{3\times3}$. The subscript of $\mathcal{A}$ reads "from FOR I to FOR A".

ii.) Rotation of γ in the *positive* direction along $\boldsymbol{e}_y^A = \boldsymbol{e}_y^B$. This transformation allows for rotation about the principal axis of the transducer. The rotation takes place in a plane *tangent* to the conduit surface, where the plane is spanned by the two vectors $\boldsymbol{e}_x^A$ and $\boldsymbol{e}_z^A$. Since the rotation takes place in the tangent plane, it must also contain the two vectors of the rotated system, $\boldsymbol{e}_x^B$ and $\boldsymbol{e}_z^B$. See Figure 1b for a visual aid. The transformation is represented by $\mathcal{A}_{AB}$.

iii.) Rotation of δ in the *positive* direction along $\boldsymbol{e}_z^B = \boldsymbol{e}_z^C$. This rotation allows the inclination of the transducer face. After the transformation, the two unit vectors $\boldsymbol{e}_x^C$ and $\boldsymbol{e}_z^C$ span a plane that contains the radiating face of the transducer. Therefore, $\boldsymbol{e}_y^C$ is the unit vector *normal* to that plane and points in the direction of the acoustic path, assuming the acoustic path is indeed incident normal to the transducing face. This unit vector may then be used to model the acoustic path in $\mathbb{R}^3$. See Figure 1b for a visual aid. The transformation is represented by the matrix $\mathcal{A}_{CB}$.

The first transformation is straight forward, the second and third are trickier to imagine, see Figure 1b for an aid. A *positive* rotation is in the sense of a mathematically positive rotation (right hand rule).

The transformation matrices can be written in terms of GIVENS rotations. Multiple definitions are possible, here we choose

$$\mathcal{A}_{AI} = \begin{pmatrix} 1 & 0 & 0 \\ 0 & \cos\alpha & \sin\alpha \\ 0 & -\sin\alpha & \cos\alpha \end{pmatrix} \tag{22}$$

$$\mathcal{A}_{BA} = \begin{pmatrix} \cos\gamma & 0 & -\sin\gamma \\ 0 & 1 & 0 \\ \sin\gamma & 0 & \cos\gamma \end{pmatrix} \tag{23}$$

$$\mathcal{A}_{CB} = \begin{pmatrix} \cos\delta & \sin\delta & 0 \\ -\sin\delta & \cos\delta & 0 \\ 0 & 0 & 1 \end{pmatrix} \tag{24}$$

Vector $\boldsymbol{r}_{\mathcal{O}P}$ of Eq. (3) is very easy described in FOR I, i.e.,

$${}_I\boldsymbol{r}_{\mathcal{O}P} = \begin{pmatrix} x \\ R\cos\beta \\ R\sin\beta \end{pmatrix} \tag{25}$$

and $\boldsymbol{r}_{T\mathcal{O}}$ is most conveniently described in B

$${}_B\boldsymbol{r}_{T\mathcal{O}} = \begin{pmatrix} 0 \\ -(R-h) \\ 0 \end{pmatrix} \tag{26}$$

where h is the distance from point T to the conduit surface along $\boldsymbol{e}_y^B$ (see Figure 1b) and R is the radius of the conduit. If $h > 0$, then point T *is inside the conduit*. If $h < 0$ then T is either *inside the conduit wall* or *outside the conduit*, where the former may rarely happen, the latter is physically not possible.

Since we are looking for ${}_C\boldsymbol{r}_{TP}$, we can now write, using Eq. (3),

$${}_C\boldsymbol{r}_{TP} = \mathcal{A}_{CB}\,{}_B\boldsymbol{r}_{T\mathcal{O}} + \mathcal{A}_{CB}\mathcal{A}_{BA}\mathcal{A}_{AI}\,{}_I\boldsymbol{r}_{\mathcal{O}P} \tag{27}$$

The acoustic path, represented by ${}_C\boldsymbol{r}_{TP}$ in the C system, is a *straight line* in $\mathbb{R}^3$. In the C system, such a line is given by

$${}_C\boldsymbol{g} = t\boldsymbol{e}_y^C \tag{28}$$

where t is an unknown parameter, i.e., the *length* of the acoustic path from point T to point P. This is the reason why we wish to describe $\boldsymbol{r}_{TP}$ in the C system. We can now write a sysem of three equations with three unknowns x, β and t related to P and two constraints γ and δ, i.e.,

$${}_C\boldsymbol{r}_{TP} = -{}_C\boldsymbol{g} \tag{29}$$

The minus sign arises from the definition of the C system, see Figure 1b. Expanding Eq. (27) and (28), the system can be written as

$$\begin{pmatrix} h\sin\delta + x\cos\gamma\cos\delta + R(c_{11}\cos\beta + c_{12}\sin\beta - \sin\delta) \\ h\cos\delta - x\cos\gamma\sin\delta + R(c_{21}\cos\beta + c_{22}\sin\beta - \cos\delta) \\ x\tan\gamma - R(\sin\alpha\cos\beta - \cos\alpha\sin\beta) \end{pmatrix} = \begin{pmatrix} 0 \\ -t \\ 0 \end{pmatrix} \tag{4}$$

with constants

$$c_{11} = \sin\delta\cos\alpha + \sin\gamma\cos\delta\sin\alpha \tag{5}$$
$$c_{12} = \sin\delta\sin\alpha - \sin\gamma\cos\delta\cos\alpha \tag{6}$$
$$c_{21} = \cos\delta\cos\alpha - \sin\gamma\sin\delta\sin\alpha \tag{7}$$
$$c_{22} = \cos\delta\sin\alpha + \sin\gamma\sin\delta\cos\alpha \tag{8}$$

B General Determination of γ and δ

In § 2.2 the angles γ and δ were determined by the two constraints that the path must lie in the plane ε and that it is aligned at the angle φ inside that plane. In general, a straight line is defined by two points. Thus, given two points T and P, one can calculate γ and δ such that the two points lie on the same path. The point T is necessarily the origin of coordinate system C, see Figure 1b. Based on these two points, the following quantities can readily be computed

$$\tan\alpha = \frac{T_z}{T_y} \tag{30}$$
$$\tan\beta = \frac{P_z}{P_y} \tag{31}$$
$$R = \sqrt{P_y^2 + P_z^2} \tag{32}$$
$$x = P_x \tag{33}$$
$$h = R - \sqrt{T_y^2 + T_z^2} \tag{34}$$

These calculations assume that P *is on the surface* of the conduit, hence, h is defined as given in Eq. (34). The assumption that P is on the surface allows these calculations in the first place and does not influence γ and δ, since T is the origin of FOR C. Once these quantities are known, the following three intermediate values may be computed

$$q_1 = \frac{x}{R} \tag{35}$$

$$q_2 = \left(\frac{\tan\alpha}{\tan\beta} - 1\right)\cos\alpha\sin\beta \tag{36}$$

$$q_3 = 1 - \frac{h}{R} - (1 + \tan\alpha\tan\beta)\cos\alpha\cos\beta \tag{37}$$

The relations for the angles γ and δ then follow from the third and first equation, respectively, of the system given in Eq. (4). That is,

$$\tan\gamma = \frac{q_2}{q_1} \tag{38}$$

$$\tan\delta = \frac{q_2}{q_3}\sin\gamma + \frac{q_1}{q_3}\cos\gamma \tag{39}$$

By introducing the two constraints discussed in § 2.2, Eq. (38) and (39) simplify to Eq. (14) and (15), respectively.